AIAA JOURNAL
Vol. 36, No. 5, May 1998

# Aspects of Numerical Uncertainties in Time Marching to Steady-State Numerical Solutions

H. C. Yee*
*NASA Ames Research Center, Moffett Field, California 94035*
and
P. K. Sweby†
*University of Reading, Whiteknights, Reading RG6 2AX, England, United Kingdom*

**Knowledge from recent advances in the understanding of global nonlinear behavior of numerical schemes is employed to isolate some aspects of numerical uncertainties in time-marching approaches to obtain steady-state numerical solutions. Strong dependence on initial data and the permissibility of spurious steady-state numerical solutions, stabilization of unstable steady states by implicit time discretizations, and convergence properties and spurious behavior of high-resolution shock-capturing schemes are discussed and illustrated with examples. The goal is to illustrate the important role that global nonlinear behavior of numerical schemes can play in minimizing sources of numerical uncertainties in computational fluid dynamics.**

## I. Introduction

SINCE the late 1980s, many computational fluid dynamics (CFD) related journals have imposed an editorial policy statement on numerical uncertainty that pertained mainly to the accuracy issue. However, the study of numerical uncertainties in practical computational physics encompasses very broad subject areas. These include but are not limited to 1) problem formulation and modeling; 2) type, order of accuracy, nonlinear stability, and convergence of finite discretizations; 3) limits and barriers of existing finite discretizations for highly nonlinear stiff problems with source terms and forcing and/or for wave propagation phenomena; 4) numerical boundary condition procedures; 5) finite representation of infinite domains; 6) solution strategies in solving the nonlinear discretized equations; 7) procedures for obtaining the steady-state numerical solutions; 8) grid quality and grid adaptations; 9) multigrids; and 10) domain decomposition (zonal or multicomponent approach) in solving large problems. See Refs. 1–9 and the references cited therein. At present some of the numerical uncertainties can be explained and minimized by traditional numerical analysis and standard CFD practices. However, such practices might not be sufficient for strongly nonlinear and/or stiff problems. Examples of this type of problem are combustion, direct numerical simulations, high-speed and reacting flows, and certain turbulence models in Navier–Stokes computations. We believe that a good understanding of the nonlinear behavior of numerical schemes being used should be an integral part of code verification and validation. See Jackson[10] for the definition of genuinely (or strongly) nonlinear problems.

The need for the study of nonlinear behavior of numerical schemes is prompted by the fact that the type of problem studied using CFD has changed dramatically over the past decade. CFD is undergoing an important transition, and it is increasingly used in nontraditional areas. But even within its field, many algorithms widely used in practical CFD were originally designed for much simpler problems, such as perfect or ideal gas flows. As can be seen in the literature, a straightforward application of well-validated CFD codes to poorly understood physical problems can lead to wrong results, excess slow convergence, or even nonconvergent solutions. Understanding the nonlinear behavior, limits, and barriers, and isolating spurious behavior of existing numerical schemes are the basic steps toward dealing with emerging disciplines. This paper addresses the time marching to the steady-state numerical solutions aspect of the subject. Yee et al.[8] addresses spurious behavior in underresolved grids and/or semi-implicit temporal discretizations for unsteady computations. Yee and Sweby[9] gives an overview of the subject for both steady and unsteady computations. We emphasize here that in our study, unless otherwise stated, we always assume the continuum (governing equations) is nonlinear.

Section II discusses some elements and issues of nonlinear behavior of numerical schemes that are relevant to time marching to the steady-state numerical solutions. Some of the subtleties discussed are necessary to illuminate and isolate the sources of numerical uncertainties due to factors such as slow convergence or nonconvergence of numerical schemes and nonlinear behavior of high-resolution shock-capturing schemes. These include spurious steady-state numerical solutions and spurious asymptotes. Here spurious numerical solutions is used to mean numerical solutions that are true solutions of the discretized counterparts but are not solutions of the underlying differential equations (DEs). The term discretized counterparts is used to mean the finite difference equations resulting from finite discretizations of the underlying DEs. Asymptotic solutions include steady-state solutions, periodic solutions, limit cycles, chaos, and strange attractors.[11,12] Section III gives an overview of selected results on nonlinear behaviors of numerical schemes. Section IV illustrates examples in CFD computations that exhibit similar spurious behavior. Because of limited space, see Ref. 9 and references cited therein for some suggestions to minimize spurious steady-state numerical solutions using knowledge of nonlinear behavior of numerical schemes. We conclude the paper with some remarks in Secs. V and VI.

## II. Elements and Issues in Time Marching to the Steady State

The time-marching approach for obtaining steady-state numerical solutions has been considered the method of choice in CFD for nearly two decades, since the pioneering work of Crocco[13] and Moretti and Abbett.[14] Moretti and Abbett used this approach to solve the inviscid supersonic flow over a blunt body without resorting to solving the steady form of partial differential equations (PDEs) of the mixed type. The introduction of efficient CFD algorithms[15–18] in the 1970s marked the beginning of numerical simulations of two-dimensional and three-dimensional Navier–Stokes equations for complex configurations. It enjoyed much success in computing a variety of weakly and moderate nonlinear fluid flow problems. For strongly nonlinear problems, the situation is more complicated. To aid the understanding of the scope of the situation, first, it is

Presented as Paper 96-2052 at the AIAA 27th Fluid Dynamics Conference, New Orleans, LA, June 18–20, 1996; received Oct. 22, 1996; revision received Jan. 29, 1997; accepted for publication Aug. 25, 1997. 

*Senior Staff Scientist, Aeronautical Technologies Division.
†Lecturer, Department of Mathematics; part of this work was performed as a Visiting Scientist, RIACS, NASA Ames Research Center.

important to identify all of the sources of nonlinearities. Second, it is necessary to isolate the elements and issues of numerical uncertainties due to these nonlinearities in time marching to the steady state.

### A. Sources of Nonlinearities in CFD

The sources of nonlinearities that are well known in CFD are due to the physics. Examples are convection, diffusion, forcing, turbulence source terms, reacting flows, combustion related problems, or any combination thereof. The less familiar sources of nonlinearities are due to the numerics. Generally, there are three major sources:

1) Nonlinearities are due to time discretizations, that is, the discretized counterpart is nonlinear in the time step. Examples of this type are Runge–Kutta methods. It is noted that linear multistep methods (LMMs) are linear in the time step (see Lambert[19] for the forms of these methods).

2) Nonlinearities are due to spatial discretizations; in this case, the discretized counterpart can be nonlinear in the grid spacing and/or the scheme. Examples of nonlinear schemes are the total variation diminishing (TVD) and essentially nonoscillatory (ENO) schemes. See Yee[20] and references cited therein for the forms of these schemes.

3) Nonlinearities are due to complex geometries, boundary interfaces, grid generation, grid refinements and grid adaptations; each of these procedures can introduce nonlinearities.

The behavior of these nonlinearities due to the numerics are not well understood. Only some preliminary development is beginning to emerge recently. The following isolates some of the elements and issues of numerical uncertainties related to these nonlinearities in time marching to the steady state. The elements and issues discussed are supported by a series of research studies reported in Refs. 9 and 21–26.

### B. Discretized Counterparts as Discrete Dynamical Systems

When we try to use numerical methods to gain insight into the fluid physics, there is an added new dimension to the overall problem. Even though we freeze the physical parameter, the resulting discretized counterparts are not just a nonlinear system of difference equations; they are also a nonlinear but discrete dynamical system on their own. From nonlinear dynamics, we know that discrete dynamical systems possess much richer dynamical behavior than the continuum dynamical systems.[21–24] These discrete dynamical systems are a function of all of the discretized parameters that are not present in the governing equations. There exist solutions of the discretized counterparts that are not solutions of the governing equations.[8,9,21–26] This is one of the key factors influencing the numerical solutions to depart from the physical ones if the governing equations are strongly nonlinear and stiff.

### C. Solving an Initial Boundary Value Problem with Unknown Initial Data

When time-marching approaches are employed to obtain steady-state numerical solutions, a boundary value problem (BVP) is transformed into an initial boundary value problem (IBVP) with unknown initial data. The time differencing in this case acts as a pseudotime. Linearized stability analysis indicates that a subset of the numerical solutions for certain ranges of the discretized parameters and boundary conditions mimic the true solution behavior of the governing equation. However, it is less known that outside these safe regions the numerical solution, depending on the initial data, does not necessarily undergo instabilities. In addition, there exist asymptotic numerical solutions that are not solutions of the continuum even inside the safe regions.[21–26] Unlike nonlinear problems, the numerical solutions of linear or nearly linear problems are independent of the discretized parameters and initial data as long as the discretized parameters are inside the stability limit [or the Courant–Friedrich–Lewy (CFL) condition]. That is, the topological shapes of these solutions remain the same within the stability limit and accuracy of the scheme for linear behavior. Yee and Sweby[22–24] illustrated the strong dependence of numerical solutions on initial data for various nonlinear model DEs. It turns out that if constant time steps are used, stability, convergence rate, and the occurrence of spurious numerical solutions are intimately related to the choice of initial data (or start-up solution).

### D. Reliability of Residual Test

Consider a quasilinear PDE of the form

$$u_t = G(u, u_x, u_{xx}, \alpha, \epsilon) \tag{1}$$

where $G$ is nonlinear in $u$, $u_x$, and $u_{xx}$. The values $\alpha$ and $\epsilon$ are system parameters. For simplicity consider a two-time-level and a $(p+q+1)$ point grid stencil numerical scheme of the form

$$u_j^{n+1} = u_j^n - H\left(u_{j+q}^n, \ldots, u_j^n, \ldots, u_{j-p}^n, \alpha, \epsilon, \Delta t, \Delta x\right) \tag{2}$$

for the PDE (1). Note that the discussion need not be restricted to explicit methods or two-time-level schemes. Let $\boldsymbol{U}^*$, a vector representing $(u_{j+q}^*, \ldots, u_j^*, \ldots, u_{j-p}^*)$, be a steady-state numerical solution of Eq. (2). When a time-marching approach such as Eq. (2) is used to solve the steady-state equation $G(u, u_x, u_{xx}, \alpha, \epsilon) = 0$, the iteration typically is stopped when the residual $H$ and/or some $\ell_2$ norm of the dependent variable $u$ between two successive iterates is less than a preselected level.

Aside from the various standard numerical errors such as truncation error, machine round-off error, etc., there is a more fundamental question of the validity of the residual test and/or $\ell_2$ norm test. If the spatial discretization happens to produce spurious steady-state numerical solutions, these spurious solutions would still satisfy the residual and $\ell_2$ norm tests in a deceptively smooth manner. Moreover, depending on the combination of time as well as spatial discretizations, it is not easy to check whether $G(u^*, u_x^*, u_{xx}^*, \alpha, \epsilon) \to 0$ even though $H(U^*, \alpha, \epsilon, \Delta t, \Delta x) \to 0$, because spurious steady states (and asymptotes) can be independently introduced by spatial and time discretizations.[25,26] This is contrary to the ordinary differential equation (ODE) case where, if $u^*$ is a spurious steady state of $du/dt = S(u)$, then $S(u^*) \neq 0$. Furthermore, if a steady state has been reached with a rapid convergence rate, it does not necessarily imply that the steady state obtained is not spurious (see Sec. III for an overview or Refs. 9 and 21 for details).

### E. Methods Used to Accelerate Convergence Process

Methods such as iterations and relaxation procedures, and/or convergence acceleration methods such as conjugate gradient methods, have been utilized to speed up the convergence process.[27] Also techniques such as preconditioning[28] and multigrid[29] combined with iteration, relaxation, and convergence acceleration procedures are commonly used in CFD. Depending on the type of PDEs, proper preconditioners can be established for the PDEs or for the particular discretized counterparts. Multigrid methods can be applied to the steady PDEs or the time-dependent PDEs. In either case, a combination of these methods can still be viewed as pseudo-time-marching methods (but not necessarily of the original PDE that was under consideration). However, if one is not careful, numerical solutions other than the desired one can be obtained in addition to spurious asymptotes due to the numerics. From here on the term time-marching approaches is used loosely to include all of the discussed methods. It is remarked that multigrid methods can be viewed as the (generalized) spatial counterpart of a variable time step control in time discretizations.

### F. Methods for Solving the Nonlinear Algebraic Equations from Implicit Methods

When implicit time discretizations are used, one has to deal with solving systems of nonlinear algebraic equations. Aside from the effect of the different methods discussed to accelerate the convergence process, we need to know how different the dynamical behavior is for the different procedures, e.g., iterative vs noniterative, in solving the resulting nonlinear difference equations (see Refs. 22–24 and the next section for a discussion).

### G. Mismatch in Implicit Schemes

It is standard practice in CFD to use a simplified implicit operator (or mismatched implicit operators) to reduce CPUs and to increase efficiency. These mismatched implicit schemes usually consist of the same explicit operator but different simplified implicit operators. The implicit time integrator is usually of the LMM type. One popular form of the implicit operator is the so-called delta formulation.[16,17]

The original logic in constructing this type of scheme is that the implicit operators act as a relaxation mechanism. However, from a dynamical system standpoint, before a steady state is reached, the nonlinear difference equations representing each of these simplified implicit operators are different from each other. They have their own dynamics as a function of the time step, grid spacing, and initial data. They also can exhibit different types of nonlinear behavior if one is solving strongly nonlinear time-dependent PDEs. Depending on the initial data, time steps, and grid spacings, when steady states have been reached, these steady states might not converge to the same steady state due to the different forms of the implicit temporal operator. On the other hand, spurious steady states can be introduced by spatial discretizations, and even if these mismatched implicit schemes converge to the same steady state, that steady state can still be spurious because the same explicit spatial operator is used. Consequently, these mismatched implicit operators can have different spurious dynamics and/or different convergence rates for the entire solution procedure[30,31](see Sec. IV and Sec. 4.3 of Yee and Sweby[9] for examples using TVD types of schemes).

### H. Nonlinear Schemes

It is well known that all of the TVD, total variation bounded (TVB) and ENO schemes[32,33] are nonlinear schemes in the sense that the final algorithm is nonlinear even for the constant-coefficient linear PDE. These types of schemes are known to have a slower convergence rate than classical shock-capturing methods and can occasionally produce unphysical solutions for certain combinations of entropy satisfying parameters and flux limiters (despite that entropy satisfying TVD, TVB, and ENO schemes can suppress unphysical solutions). See Yee[20] for a summary of the subject. The second aspect of these nonlinear schemes is that even if the numerical method is formally of more than first order and if the approximation converges, the rate may still be only first order behind the shock (not just around the shock). This can happen for systems where one characteristic may propagate part of the error at a shock into the smooth domain. Engquist and Sjogreen[34] illustrate this phenomena with examples (see Sec. IV.B for a discussion). The third aspect of these higher-order nonlinear schemes is their true accuracy away from shocks (see Donat,[35] Casper and Carpenter,[36] and Yee and Sweby[9] for a discussion).

### I. Schemes That are Linear vs Nonlinear in $\Delta t$

The obvious classification of time-accurate schemes for time-marching approaches to the steady state are explicit, implicit, and hybrid explicit and implicit methods. A less-known classification of numerical schemes for time-marching approaches is the identification of schemes that are linear or nonlinear in the $\Delta t$ parameter space when applied to nonlinear DEs. As mentioned before, all LMMs (explicit or implicit) are linear in $\Delta t$ and all multistage Runge–Kutta methods are nonlinear in $\Delta t$. Lax–Wendroff and MacCormack type of nonseparable full discretizations also are nonlinear in $\Delta t$. A desirable property for a scheme that is linear in $\Delta t$ is that, if the numerical solution converges, its steady-state numerical solutions are independent of the time step. On the other hand, the accuracy of the steady-state numerical solutions (also for time-accurate numerical solutions) depends on $\Delta t$ if the scheme is nonlinear in $\Delta t$. Certain of these types of schemes are more sensitive to $\Delta t$ than others. For example, Lax–Wendroff and MacCormack methods are more sensitive than the Lerat and Sides variant.[37] A less-known property of schemes that are nonlinear in $\Delta t$ is that this type of scheme has an important bearing on the existence of spurious steady-state numerical solutions due to time discretizations. Although schemes such as LMMs are immune from exhibiting spurious steady-state numerical solutions, as seen in Yee and Sweby,[22–24] a wealth of surprisingly nonlinear behavior of implicit LMMs that had not been observed before were uncovered by the nonlinear study (see Yee and Sweby[9] and the next section for a review).

### J. Adaptive Time Step Based on Local Error Control

It is a standard practice in CFD to use local time step (varied from grid point to grid point using the same CFL) for nonuniform grids. However, except in finite element methods, adaptive time step based on local error control is rarely use in CFD. Adaptive time step is builtin for standard ODE solver computer packages.[38] It enjoyed much success in controlling accuracy and stability for transient (time-accurate) computations. The issue is: to what extent does this adaptive local error control confer global properties in long time integration of time-dependent PDEs? Can one construct similar error control that has guaranteed and rapid convergence to the correct steady-state numerical solutions in the time-marching approaches for time-dependent PDEs? Section III.C summarizes the status of this subject.

### K. Nonunique Steady-State Solutions of Nonlinear DEs vs Spurious Asymptotes

The phenomenon of generating spurious steady-state numerical solutions (or other spurious asymptotes) by certain numerical schemes is often confused with the nonuniqueness (or multiple steady states) of the governing equation. In fact, the existence of nonunique steady-state solutions of the continuum can complicate the numerics tremendously and is independent of the occurrence of spurious asymptotes of the associated scheme. But, of course, a solid background in the theory of nonlinear ODEs and PDEs and their dynamical behavior is a prerequisite in the study of the dynamics of numerical methods for nonlinear PDEs. A good understanding of the subject can shed some light on the controversy about the true existence of multiple steady-state solutions through numerical experiments for certain flow types of the Euler and/or Navier–Stokes equations.

## III. Overview of Selected Results

In a series of papers,[8,21–26,39–41] the nonlinear dynamics of finite discretizations for constant time steps and fixed or adaptive grid spacings was studied using tools from dynamical systems theory. The approach was to take continuum nonlinear model ODEs and PDEs with known analytic solutions, discretize them according to various standard numerical methods, and apply techniques from discrete dynamical systems theory to analyze the nonlinear behavior of the resulting nonlinear difference equations. Particular attention was paid to the isolation of the different nonlinear behavior and spurious dynamics due to some of the numerical uncertainties that were observed in practical CFD computations. The numerical schemes considered for these nonlinear model ODEs and PDEs were selected to illustrate the following different nonlinear behavior of numerical methods: 1) occurrence of stable and unstable spurious asymptotes above the linearized stability limit of the scheme (for constant time steps), 2) occurrence of stable and unstable spurious steady states below the linearized stability limit of the scheme (for constant time steps), 3) stabilization of unstable steady states by implicit and semi-implicit methods, 4) interplay of initial data and time steps on the occurrence of spurious asymptotes, 5) interference with the dynamics of the underlying implicit scheme by procedures in solving the nonlinear algebraic equations (resulting from implicit discretization of the continuum equations), 6) dynamics of the linearized implicit Euler scheme solving the time-dependent equations vs Newton's method solving the steady equation, 7) spurious dynamics independently introduced by spatial and time discretizations, 8) convergence problems and spurious behavior of high-resolution shock-capturing methods, 9) numerically induced and suppressed chaos and numerically induced chaotic transients, and 10) spurious dynamics generated by grid adaptations.

Because of the complexity of the nonlinear analysis, a logical breakdown of the key nonlinear studies can consist of 1) initial value problems (IVPs) of explicit and implicit temporal discretizations, 2) BVPs of linear and nonlinear spatial discretizations, 3) IBVPs of time-accurate schemes, 4) IBVPs of time marching to the steady state, and 5) nonlinearities introduced by grid generation, grid adaptation and complex geometries.

Spurious behavior of spatial discretizations for BVPs was discussed in Refs. 9 and 21. Spurious behavior of IBVPs for time-accurate schemes was discussed in Refs. 8 and 9. To gain an understanding of the nonlinear behavior of time discretizations without the influence from the spatial discretizations, Refs. 21–24 studied commonly used time discretizations for nonlinear ODE models. For the purpose of this paper, the next section summarizes some aspects

of the nonlinear behavior of time discretizations for constant time steps. We remark that time-marching approaches to the steady state rarely employed constant time steps but rather use local time steps based on the Jacobian of the curvilinear grid transformation and the CFL constraint. However, a basic understanding of the dynamics of constant time steps is essential to improve the solution procedures and to the understanding of the dynamics of variable time steps based on local error control.[42,43]

### A. Nonlinear Behavior of Time Discretization

The global asymptotic nonlinear behavior and bifurcation phenomena for the explicit Euler method, five different multistage Runge–Kutta methods (modified Euler, improved Euler, Heun, Kutta, and fourth-order methods), two- and three-step predictor–corrector methods, Adams–Bashforth method, a semi-implicit method, and four implicit LMMs (implicit Euler, trapezoidal, three-point backward differentiation and midpoint implicit methods) with four ways for solving the nonlinear algebraic equations are compared for different nonlinear model ODEs in Refs. 21–24. The emphasis is on the interplay of initial data and time steps on the occurrence of spurious asymptotic numerical solutions. The four ways for solving the nonlinear algebraic equations considered are the noniterative linearized form, simple iteration, Newton, and modified Newton methods. The five multistage Runge–Kutta methods and the predictor–corrector methods are nonlinear in the discretized parameter space $\Delta t$, whereas the four implicit LMMs are linear in $\Delta t$.

In general, some of the second-order or higher explicit Runge–Kutta methods can introduce spurious steady states below the linearized stability limit of the schemes whereas implicit LMMs can stabilize an unstable steady state of the governing equations. The dynamics of these time discretizations differ significantly from each other, and the different methods of solving the resulting nonlinear algebraic equations are very different from each other because different numerical methods and solution procedures result in entirely different nonlinear difference equations. For systems of nonlinear ODEs, the steady-states numerical solutions can change types as the time step is varied for the studied unconditionally stable implicit LMMs. An unstable steady state of the governing equation can become stable and can, e.g., change from a saddle to a stable or unstable node (for the same system parameter). One major consequence of this behavior is that part or all of the flow pattern can change type as the discretized parameter is varied. Even though LMMs preserve the same number but not the same types of steady states as the underlying DEs, LMMs can introduce spurious asymptotes other than spurious steady states. Consequently, for given initial data and two finite but different $\Delta t$ that are below the linearized stability limit of the scheme, their numerical solutions might converge to two different solutions even if no spurious stable steady-state numerical solution is introduced by the scheme and the initial data are physically relevant. The source of the behavior is due to the existence of unstable spurious asymptotes, stable asymptotes other than steady states, or stabilization of unstable steady states. In other words, for a given $\Delta t$ below the linearized stability limit, the numerical solution can, depending on the initial data, 1) converge to the correct steady state, 2) converge to a different steady state, 3) converge to a spurious periodic solution or limit cycle, 4) stabilize an unstable steady state of the governing equations, 5) yield spurious asymptotes other than solution 1–4, or 6) diverge, even though the initial data are physically relevant.

### B. Strong Dependence on Initial Data

One of the key concepts in understanding the interplay of initial data and time steps on the occurrence of spurious asymptotes is basins of attraction. The basin of attraction of an asymptote (for the DEs or their discretized counterparts) is a set of all initial data asymptotically approaching that asymptote. In other words, a basin of attraction tells which initial data lead to which asymptotes. For each asymptote of the DE and the underlying difference equation, the terms *exact basin of attraction* and *numerical basin of attraction* refer to the basin of attraction of the DE and basin of attraction of the underlying discretized counterpart, respectively. For a constant time step, spurious asymptotic numerical solutions, if they exist, occupy their own numerical basins of attraction. The size of these basins of attraction varies from one time step to another and, consequently, interfere with the size of the numerical basins of attraction of the true steady states.

In Refs. 22–26, the authors showed how numerical basins of attraction can help in gaining a better understanding of the global asymptotic behavior of numerical solutions for nonlinear DEs. In particular, they showed how in the presence of spurious asymptotes, the basins of the true stable steady states can be segmented by the basins of the spurious stable and unstable asymptotes. One major consequence of this phenomenon, which is not commonly known, is that this spurious behavior can result in a dramatic distortion and, in most cases, a dramatic shrinkage and segmentation of the basin of attraction of the true solution for finite time steps. Such distortion, shrinkage, and segmentation of the numerical basins of attraction will occur regardless of the stability of the spurious asymptotes. In other words, the size of the domain of initial data approaching the underlying asymptotes changes with the time step even when one operates with time steps that are below the linearized stability limit. Studies showed that all of the four implicit LMMs exhibit a drastic distortion but less shrinkage of the basin of attraction of the true solution than explicit methods. As is the case for standard explicit methods, but in some cases with smaller $\Delta t$, the implicit LMMs exhibit enlargement of the basins of attraction of the true solution. Such enlargement occurs when $\Delta t$ is small or in the vicinity of the stability limit of standard explicit method counterparts.

Although unconditionally stable implicit methods allow theoretically large $\Delta t$ (in the order of $10^3$–$10^6$), the numerical basins of attraction for large $\Delta t$ sometimes are so fragmented and/or so small that the safe (or practical) choice of $\Delta t$ is slightly larger or comparable to the stability limit of standard explicit methods (but with a much larger numerical basin of attraction than their explicit method counterparts). In general, if one uses a $\Delta t$ that is a fraction of the stability limit, one has a higher chance of convergence to the correct asymptote because the numerical basins of attraction more closely resemble the exact basin of attraction. Thus, for the same $\Delta t$, unconditionally stable LMMs are safer to use than explicit methods. Some of the phenomena observed in our study can be used to explain the root of why one cannot achieve the theoretical linearized stability limit of the typical explicit and implicit time discretizations in practice when solving strongly nonlinear DEs, e.g., in CFD. These behaviors indicate that it is plausible to rely on time marching to the steady-state numerical solutions with unknown initial data. An important implication of the basin of attraction study is that associated with static initial data, stable spurious solutions, if they exist, are also very likely to be stable under static initial data perturbations.

### C. Suppression of Spuriosity by Error Control

The preceding sections discussed the spurious behavior of long time integrations of IVPs of nonlinear ODE solvers for constant step sizes. The use of adaptive step size based on local error control for implicit methods was studied by Dieci and Estep.[42] Dieci and Estep concluded that for the implicit LMMs with local step size error control and depending on the method of solving the resulting nonlinear algebraic equations, spurious behavior can occur. Our study on two-variable step size control methods[22] indicated that one shortcoming is that the size of $\Delta t$ needed to avoid spurious dynamics is impractical to use. Aves et al.[43] addressed the heart of the question of whether local error control confers global properties of steady states of the IVP of autonomous ODEs using adaptive Runge–Kutta type methods.

The work of Aves et al. is concerned with long-term behavior and global quantities of general explicit Runge–Kutta methods with step size control for autonomous ODEs. They believed that the limit $t_n \to \infty$ is more relevant than the limit of the variable step sizes $\Delta t \to 0$. They studied spurious steady states that persist for arbitrarily small error tolerances $\tau$. This type of adaptive Runge–Kutta method usually consists of primary and secondary Runge–Kutta methods of different order. Their main result is positive. When standard local error control is used, the chance of encountering spuriosity is extremely small. For general systems of ODEs, the constraints imposed by the error control criterion make spuriosity extremely unlikely. For scalar problems, however, the mechanism by which the algorithm succeeds is indirect; spurious steady states are not

removed, but those that exist are forced by the step size selection mechanism to be locally repelling [with the relevant eigenvalues behaving as $O(1/\tau)$].

David Griffiths is currently working on the application to hyperbolic PDEs. His preliminary results (1996) showed it is by no means clear at the moment whether stable spurious solutions may be eliminated. The difference is that, unlike physical problems governed by nonlinear ODEs, nonlinear PDEs may have wavelike solutions rather than steady states due to the spatial derivatives.

### D. Nonlinear Behavior and Spurious Dynamics of Full Discretizations

A similar study for selected finite difference methods in the framework of a nonlinear model scalar reaction-convection PDE was reported in Lafon and Yee.[25,26] In their study, they also investigated the possible connection of incorrect propagation speeds of discontinuities with the existence of some stable spurious steady-state numerical solutions. The effect of spatial as well as time discretizations on the existence and stability of spurious steady-state numerical solutions was discussed. They also investigated the effect of different methods of numerical evaluation of the nonlinear source term on stability and accuracy of the overall scheme. They found that spatial and time discretizations and numerical treatment of the source term can independently introduce spurious dynamics to the overall scheme. Some of the spurious behavior observed in time discretizations in Refs. 21–24 were also observed in this PDE case.

### E. Spurious Dynamics in Time-Accurate Computations

In the examples chosen by Lorenz,[44] he showed that numerical chaos always precedes divergence of a computational scheme. He suggested that computational chaos is a prelude to computational instability. Poliashenko and Aidun[45] showed that this is not a universal scenario. Yee et al.[21] and Yee and Sweby[22–24] showed that numerics can introduce chaos. Using a simple example, Corless[46,47] showed that numerics can suppress chaotic solutions. The work of Poliashenko and Aidun[45] also discussed spurious numerics in transient computations. Adams[48] discussed spurious chaotic phenomena in astrophysics and celestial mechanics. He showed that the source of certain observed chaotic numerical solutions might be attributed to round-off errors. Adams also discussed the use of interval arithmetics (interval mathematics or enclosure methods) to avoid this type of spurious behavior. Moore et al.[49] discussed the reliability of numerical experiments in thermosolutal convection. Keener[50] discussed the uses and abuses of numerical methods in cardiology. Yee et al.[8] discussed spurious behavior in practical time-accurate CFD simulations.

In addition to the inherent chaotic and chaotic transient behavior in some physical systems, numerics can independently introduce and suppress chaos as well as chaotic transients. Section 5.1 of Yee and Sweby[9] shows a practical example of a numerically induced chaotic transient near the onset of turbulence in a direct numerical simulation of a three-dimensional channel flow studied by Keefe in 1996. Loosely speaking, a chaotic transient behaves like a chaotic solution.[51] A chaotic transient can occur in a continuum or a discrete dynamical system. One of the major characteristics of a numerically induced chaotic transient is that if one does not integrate the discretized equations long enough, the numerical solution has all of the characteristics of a chaotic solution. The required number of integration steps might be extremely large before the numerical solution can get out of the chaotic transient mode. In addition, standard numerical methods, depending on the initial data, usually experience drastic reductions in step size and convergence rate near a bifurcation point (in this case the transition point) in addition to the bifurcation points due solely to the discretized parameters (see Yee and Sweby[9,22] for a discussion). Consequently, the possible numerically induced chaotic transient is especially worrisome in direct numerical simulations (DNS) of transition from laminar to turbulent flows. Except for special situations, it is impossible to compute the exact transition point by mere DNS of the Navier–Stokes equations. Even away from the transition point, this type of numerical simulation is already very CPU intensive and the convergence rate is usually rather slow. Because of the limited computer resources, the numerical simulation can result in chaotic transients indistinguishable from sustained turbulence, yielding a spurious picture of the flow for a given Reynolds number. Consequently, it casts some doubt on the reliability of numerically predicted transition points and chaotic flows.[8,9] It also influences the true connection between chaos and turbulence.

## IV. Spurious Dynamics in Steady-State Computations

Any CFD practitioner would agree that making a time-marching CFD computer code converge efficiently to a correct steady state for a new physical problem, which was previously not understood, is still an art rather than a science. Most often, even after tuning the code, one might still encounter one or more symptoms such as blowup, nonconvergence, and unphysical or slow convergence of the numerical solution. Some of these phenomena have been reported in conference proceedings and reference journals, but the majority have been left unreported. Although these behaviors might be caused by factors such as poor grid quality, underresolved grids, improper numerical boundary conditions, etc., most often they can be overcome by employing standard procedures such as using physical guidelines, grid refinement, improved numerical boundary treatments, reducing the time step in half, and using more than one scheme to double check if the numerical solution is accurate and physically correct. However, these standard practices alone may sometimes be misleading, not possible, e.g., too CPU intensive, or inconclusive due to the various numerical uncertainties (see Secs. I and III) that can be attributed to the overall solution process. Consequently, isolation of the sources of numerical uncertainties is of fundamental importance. Section III isolates some of the spurious numerics for elementary models. Complementing the phenomena observed in Sec. III, this section illustrates examples from CFD computations. We concentrate mainly on the convergence issues that are contributed by the spurious dynamics that are inherent in the schemes.

### A. One-Dimensional Chemically Relaxed Nonequilibrium Flow Model

This section discusses the analysis of numerical basins of attraction for the simulation of a one-dimentional chemically relaxed nonequilibrium flow model for an ($N_2$, N) mixture.[52] This type of flow is encountered in various physical situations, such as shock tube experiments (the mixture behind the shock being in a highly nonequilibrium state) or a high-enthalpy hypersonic wind tunnel. Under these assumptions the steady one-dimensional Euler equations can be reduced to a single ODE,

$$\frac{dz}{dx} = S(\rho, T, z) \tag{3}$$

where $z$ is the mass fraction of the $N_2$ species, $\rho$ is the density of the mixture, and $T$ is the temperature. There are two algebraic equations for $\rho$ and $T$. This system consists of a large disparity in the range of parameter values and is stiff and highly nonlinear.

The derivation of the model is as follows. The one-dimensional steady Euler equations for a reacting ($N_2$, N) mixture are

$$\frac{d}{dx}(\rho_{N_2} u) = \dot{w}_{N_2} \tag{4a}$$

$$\frac{d}{dx}(\rho u) = 0 \tag{4b}$$

$$\frac{d}{dx}(\rho u^2 + p) = 0 \tag{4c}$$

$$\frac{d}{dx}[u(E + p)] = 0 \tag{4d}$$

where Eq. (4a) is the balance equation for the $N_2$ species and $\dot{w}_{N_2}$ is the production rate of the $N_2$ species with density $\rho_{N_2}$. The variables $\rho$, $u$, $E$, and $p$ are density, velocity, total internal energy per unit volume, and pressure, respectively.

The production rate $\dot{w}_{N_2}$ of species $N_2$ is the sum of the production rates for the two reactions

$$N_2 + N_2 \rightleftharpoons 2N + N_2 \tag{5a}$$

$$N_2 + N \rightleftharpoons 2N + N \tag{5b}$$

and is computed using Park's model[53] that has been used extensively for hypersonic computations (see the 1991 Workshop on Hypersonics[54] for some discussion). These reaction rates involve an equilibrium constant $K_{eq}$, which is determined by a polynomial fitting to experimental data and, as such, is only valid for a certain range of temperatures. In particular, a cutoff value has to be introduced for low temperatures, a typical choice being $T_{min} = 1000$ K (Ref. 55).

The systems (4) and (5) must be closed by a thermodynamic representation of the mixture. Here a simple model, with no vibrational effects, has been chosen. The details have been omitted for brevity.

Equations (4b–4d) simply integrate to give

$$\rho u = q_\infty \tag{6a}$$

$$\rho u^2 + p = P_\infty \tag{6b}$$

$$H = (E + p)/\rho = H_\infty \tag{6c}$$

where $H$ is the total enthalpy and $q_\infty$, $P_\infty$, and $H_\infty$ are all constants. Finally, denoting the mass fraction of the $N_2$ species by

$$z = \rho_{N_2}/\rho \tag{7}$$

and using Park's reaction rate model[54] and the thermodynamic closure, Eq. (3) can be written as

$$\frac{dz}{dx} = S(\rho, T, z)$$

$$= \frac{1}{M_1 q_\infty}\rho^2 T^B \exp\left(-\frac{\theta}{T}\right)\left[\alpha A_1 z(1-z)^2 - A_1 z^2 + 2\alpha A_2(1-z)^3 - 2A_2 z(1-z)\right] \tag{8a}$$

where

$$\alpha = \frac{4\rho}{M_1 K_{eq}}$$

$$K_{eq} = 10^6 \exp\left[c_1 + c_2 Z + c_3 Z^2 + c_4 Z^3 + c_5 Z^4\right] \tag{8b}$$

$$Z = \frac{10^4}{T}$$

The density $\rho$ is obtained from

$$q_\infty^2(8 - 2z)(1/\rho)^2 - (10 - 3z)P_\infty(1/\rho) + 2(2 - z)\left[H_\infty - (1 - z)e_2^0\right] = 0 \tag{8c}$$

the temperature $T$ from

$$T = \frac{M_1 p}{R(2 - z)\rho} \tag{8d}$$

and the pressure from

$$p = P_\infty - \left(q_\infty^2/\rho\right) \tag{8e}$$

The model uses the constants

$$\begin{bmatrix} c_1 = 3.898 \\ c_2 = -12.611 \\ c_3 = 0.683 \\ c_4 = -0.118 \\ c_5 = 0.006 \\ M_1 = 28 \times 10^3 \end{bmatrix} \qquad \begin{bmatrix} A_1 = 3.7 \times 10^{15} \\ A_2 = 1.11 \times 10^{16} \\ B = -1.6 \\ \theta = 1.132 \times 10^5 \\ e_2^0 = 3.355 \times 10^7 \\ R = 8.3143 \end{bmatrix}$$

The input parameters $q_\infty$, $P_\infty$, and $H_\infty$ are set equal to 0.0561, 158,000, and $27.4 \times 10^6$, respectively. A limitation of the model is $T > T_{min} = 1000$ K. The acceptable root of Eq. (8c) is taken to be real and positive. In addition, solutions are nonphysical if $z \notin [0, 1]$, if $p < 0$, or if $\rho$ is complex.

In the integration of Eq. (3), the spatial variable $x$ acts as a time-like variable. The asymptotic state is the equilibrium state given by $S(\rho, T, z) = 0$. Equation (8a) was integrated using the Euler, modified Euler [a second-order Runge–Kutta (R–K 2)], improved Euler (R–K 2), Heun [a third-order Runge–Kutta (R–K 3)], Kutta (R–K 3), and fourth-order Runge–Kutta (R–K 4) schemes.

There are two strategies possible when implementing these schemes. One is to freeze the values of $\rho$ and $T$ at the beginning of each step when calculating $S(\rho, T, z)$ at the intermediate stages. The other is to update the values at each evaluation of the function $S$. The results presented here employ the latter strategy because this is the more proper implementation; however, it is interesting to note (see following discussion) that results obtained by freezing $\rho$ and $T$ for intermediate calculations exhibit a slightly richer dynamic structure.

In each case, the computations were performed for a range of initial $z$ and integration steps $\Delta x$. For each fixed $\Delta x$ and each initial datum, the discretized equations were preiterated 1000 steps before a full bifurcation diagram (of the asymptotic states) together with basins of attraction were produced. The preiterations are necessary for the solutions to settle to their asymptotic values. To obtain a bifurcation diagram with numerical basins of attraction superimposed, the preselected domain of initial data and the preselected range of the $\Delta x$ parameter are divided into 256 or 512 equal increments. We keep track where each initial datum asymptotically approaches, and color code each basin according to the individual asymptotes. Figures 1 show the results obtained from these computations. Because for each $\Delta x$, only two distinct basins of attraction are present for all of the computations, only the grey-scale version of these plots are shown. In all of these plots the shaded region denotes the basin of attraction in which combinations of initial upstream input $z$ values and step size $\Delta x$ converge to the stable asymptotes of the discretized equations, shown by the solid black line or black dots. The unshaded regions indicate regions of upstream initial input, where the combinations of upstream input $z$ and $\Delta x$ do not converge or converge to a nonphysical solution of the problem [see condition following Eq. (8c)]. As can be seen in all cases, there is a drastic reduction in the basins of attraction with just a slight increase in the grid spacing. (The axis scale is $10^{-5}$.) Note that the allowable upstream initial input (exact basin of attraction) for the governing equation (3) is $0 \le z \le 1$.

The explicit Euler scheme (Fig. 1a) obtains the correct equilibrium state up to its linearized stability limit, where there is a very small region of period two spurious solutions before it diverges. Similar behavior is observed for the improved Euler (Fig. 1c) and Kutta (Fig. 1f) schemes, the latter also exhibiting a much more constricted basin of attraction for any given $\Delta x$. The Heun scheme (Fig. 1d) exhibits a distinct region where stable spurious periodic solutions occurred just above the linearized stability limit.

As is typical with the modified Euler scheme (Fig. 1b) a transcritical bifurcation occurs at its stability limit, which leads to a spurious ($\Delta x$-dependent) solution near the stability limit. Note also the solid line at about $z = 0.25$ down on the plot, outside of the shaded region. This appears to be an unstable feature picked up by our method of asymptotic equilibrium state detection (comparison of initial data with the 1000th iterate) and is unlikely to arise in practical calculations unless the initial data are on this curve. The R–K 4 scheme (Fig. 1e) also exhibits a transcritical bifurcation at the linearized stability limit; however, this is discernible more by the sudden narrowing of the basin of attraction because the spurious asymptotic state varies only slightly with $\Delta x$.

If the values of $\rho$ and $T$ are frozen for intermediate calculations, the dynamics are somewhat modified. All schemes with the exception of the explicit Euler have a slightly larger basin of attraction for values of $\Delta x$ within the stability limit and all schemes have period two behavior at the stability limit, there being no transcritical bifurcations for any of the schemes. The modified Euler scheme also has embedded period doubling and chaotic behavior below the linearized stability limit. For the classification of bifurcation points and their effects on the existence of spurious asymptotic numerical solutions, see Ref. 9, 21, or 56.

These computations illustrate the sensitivity of the allowable upstream initial inputs to the slight increase in the grid spacing. In other words, with a slight increase in the grid spacing, the allowable upstream initial inputs quickly become numerically unphysical. Although the dynamical behavior of the studied schemes is perhaps not as rich as in some of simple examples discussed in Refs. 21–26, spurious features can still occur in practical calculations so care must be taken in both computation and interpretation. The computations using implicit LMMs are reported in Ref. 8.

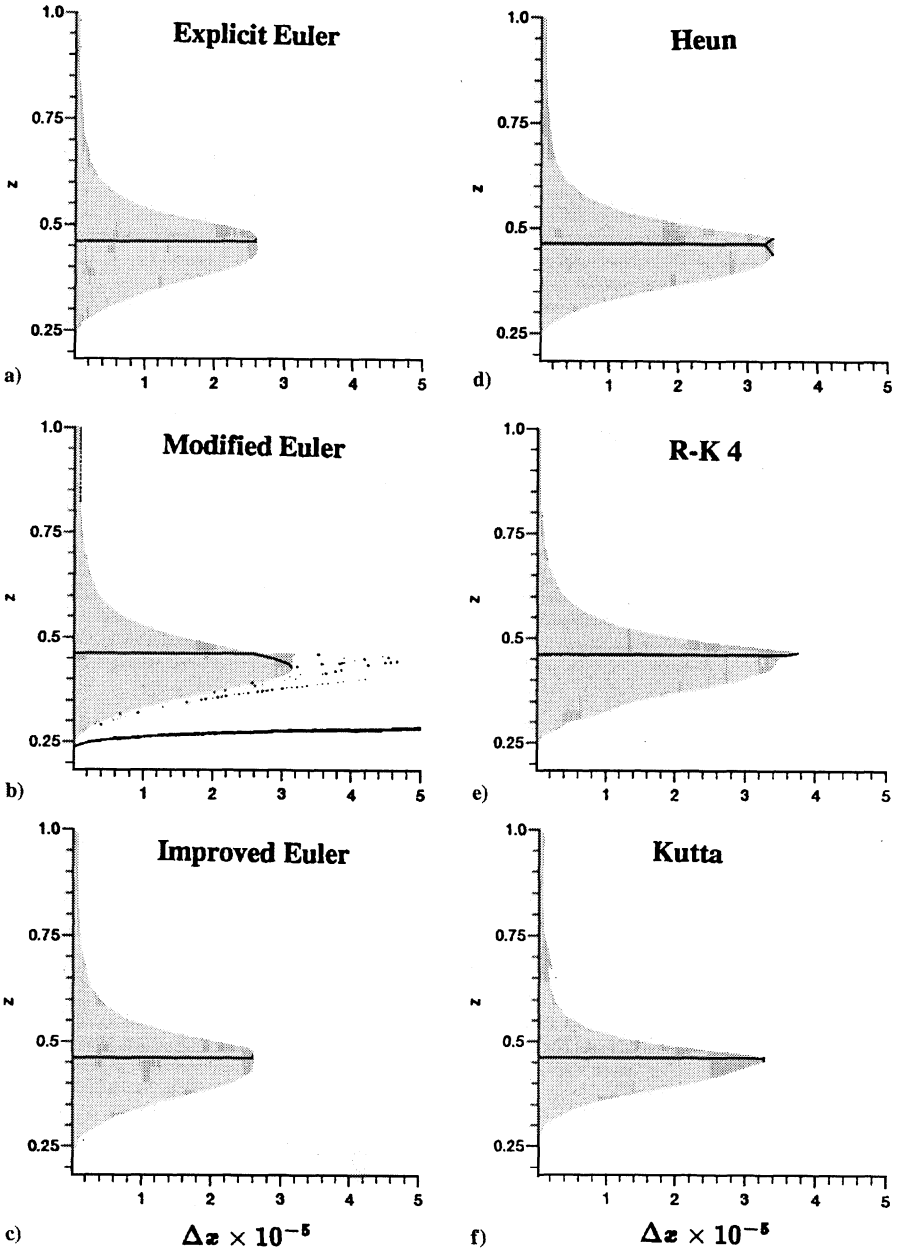


**Fig. 1 Bifurcation diagrams of fixed points of three-species reacting flow model.**

### B. Convergence Rate and Spurious Dynamics of High-Resolution Shock-Capturing Schemes

We have seen in Sec. III elementary examples and references cited therein on how the proper choice of initial data and the step size combination can avoid spurious dynamics. Yet for other combinations the numerical solutions can get trapped in a spurious limit cycle. We have also seen that the convergence rates of the schemes are greatly affected by the step sizes that are near bifurcation points. Here we include the dynamics of full discretization of two nonlinear PDE examples. The spatial discretizations are of the high-resolution shock-capturing type (nonlinear schemes). This includes TVD and ENO schemes. Section IV.B.1 discusses how this nonlinear scheme affects the convergence rate of systems of hyperbolic conservation laws. Section IV.B.2 illustrates the existence of spurious asymptotes due to the various flux limiters that are builtin to TVD schemes.

#### *1. Convergence Rate for Systems of Hyperbolic Conservation Laws*

This section summarizes the results of Engquist and Sjogreen[57] and Sjogreen (1996). These results concern the convergence rate for discontinuous solutions of a system of nonlinear hyperbolic conservation laws. For a scalar nonlinear conservation law, the characteristics point into the shock. According to the linear theory of Kreiss and Lundqvist,[58] dissipative schemes damp out errors propagating backwards against the direction of the characteristics. Thus, it is reasonable to expect that the locally large errors at the shock stay in a layer near the shock. In numerical experiments we usually obtain $\mathcal{O}(h^p)$ convergence away from the shock with difference schemes of formally $p$th order.

For the systems case, the scalar conservation law reasoning cannot be applied. In this case other families of characteristics intersecting the shock cause the situation to be more involved. Thus, it is possible that the large error near the shock propagates out into the entire post-shock region by following a characteristic that emerges from the shock.

This effect cannot be seen in a simple scalar Riemann problem (problem with jump initial data), because exact global conservation determines the postshock states. The system model problem, taken from Engquist and Sjogreen,[57]

$$u_t + (u^2/4)_x = 0, \qquad -\infty < x < \infty, \qquad 0 < t \tag{9a}$$

$$v_t + v_x + g(u) = 0, \qquad g(u) = (u+1)(u-1)\left(\tfrac{1}{2} - u\right) \tag{9b}$$

gives an example of propagation of large errors. The function $g(u)$ has the properties $g(1) = g(-1) = g(\frac{1}{2}) = 0$, and $g(u) \neq 0$ for $-1 < u < 1$ except at $u = \frac{1}{2}$. The initial data was given as

$$u_0(x) = \begin{cases} 1 & x \leq 0, \\ -1 & x > 0, \end{cases} \qquad v_0(x) = 1 \tag{9c}$$

so that the exact solution of the $u$ equation is a steady shock. The eigenvalues of the Jacobian matrix of the flux $(u^2/4, v)^T$ for Eq. (9) are $\lambda_1 = u/2$ and $\lambda_2 = 1$. The eigenvalue $\lambda_1 = u/2$ corresponds to a strictly nonlinear field, and $\lambda_2 = 1$ corresponds to a linearly degenerate field.

With these initial data [Eq. (9c)], it gives rise to a steady 1-shock, with the 1-characteristics having a slope $\frac{1}{2}$ to the left of the shock and a slope $-\frac{1}{2}$ to the right of the shock. These thus intersect the shock when time increases. The 2-characteristics of the linear field have slope 1 on both sides of the shock. These characteristics thus enter the shock from the left and exit to the right. The $v$ component of the solution is passively advected along the 2-characteristics. When these characteristics exit from the shock at $x = 0$, an error, coming from poor accuracy locally at the shock, is picked up and advected along with the solution into the domain $x > 0$. The shock curve $x = 0$ ( in the $x$–$t$ plane ) acts as an inflow boundary for the domain $x > 0$. The error coming from the shock is similar to an error in given inflow data and is, therefore, not affected by the numerical method used in the interior of the domain. Thus it is not surprising that this error is of first order, even when the equation is solved by a method of higher formal order of accuracy.

Figure 2 shows the numerical solution, computed by a second-order accurate ENO method using 50 grid points at the time $T = 5.68$. The points in the shock give a large error, which is coupled to the $v$ equation through $g(u)$. The exact solution for $v$ is 1. Numerical investigation of the convergence rate of the error in $v$ to the right

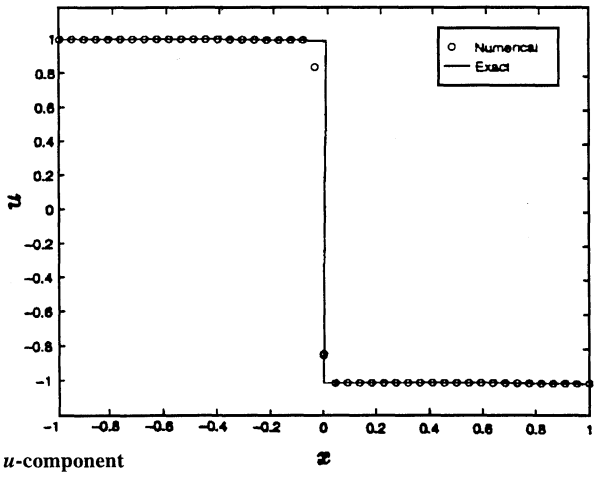


$u$-component

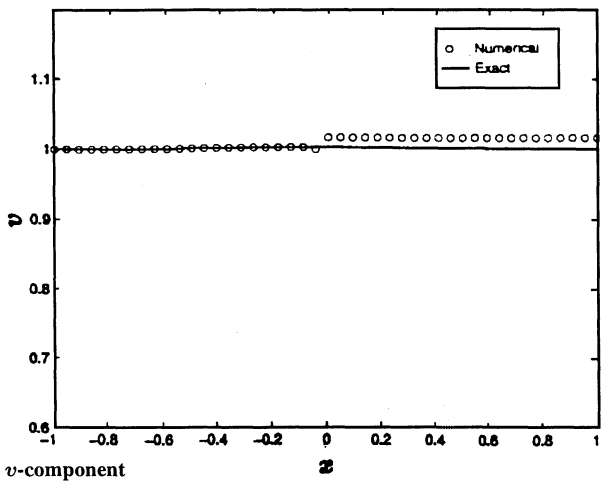


$v$-component

**Fig. 2 For a second-order ENO scheme, $u$ and $v$ components of Eq. (9).**

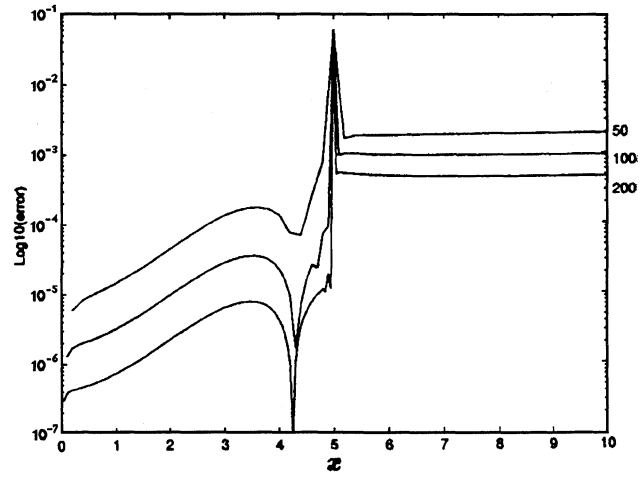


**Fourth-order ENO scheme**

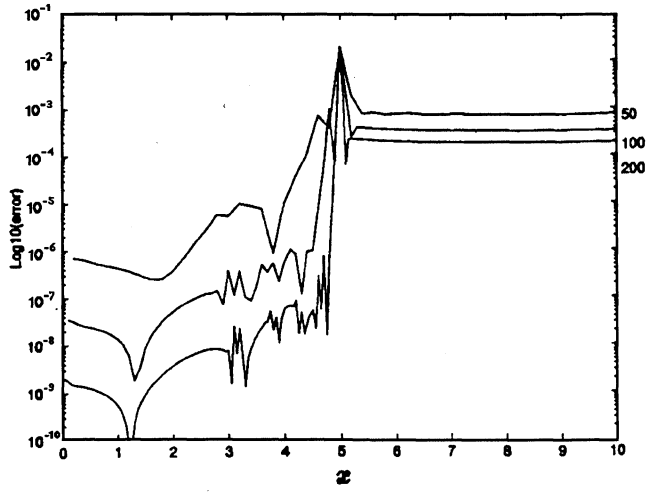


**Second-order TVD scheme**

**Fig. 3 Error in momentum of Eq. (9).**

gave the exponent 1.047. Thus, one has first-order convergence for this second-order accurate method.

Similar effects can be seen in computing the quasi-one-dimensional nozzle flow. Engquist and Sjogreen[34] computed the solution on the domain $0 < x < 10$ for a nozzle with the following cross-sectional area variation:

$$A(x) = 1.398 + 0.347 \tanh(0.8x - 4) \tag{10}$$

This problem is studied in Yee et al.[59] for a class of explicit and implicit TVD schemes. The solution has a steady shock in the middle of the domain. Figure 3 shows the error in momentum for the steady-state solution on grids of 50, 100, and 200 points for a fourth-order ENO scheme and a second-order TVD scheme. For the fourth-order method, the convergence exponent is 3.9 before the shock and 1.0 after the shock, when going from 100 to 200 points. For the second-order TVD the same quantities have the values 2.2 and 1.1, respectively.

Sjogreen recently conducted the same numerical study for the two-dimensional compressible Euler equations for a supersonic flow past a disk with Mach number 3. The equations were discretized by a second-order accurate uniformly nonoscillatory (UNO) scheme,[32] which, unlike TVD schemes, is formally second order everywhere including smooth extrema. He computes the error in entropy along the stagnation line for the steady-state solution on grids with $33 \times 17$, $65 \times 33$, and $129 \times 65$ grid points. The result is shown in Fig. 4, where the error and convergence exponent in the region behind the bow shock are plotted. The convergence exponent is between the $65 \times 33$ and the $129 \times 65$ grids. The disk has radius 0.5, and it is centered at the origin, which means that the line is attached to the wall for $-0.5 < x$. A convergence exponent of 1.5 is observed for this formally second-order method.

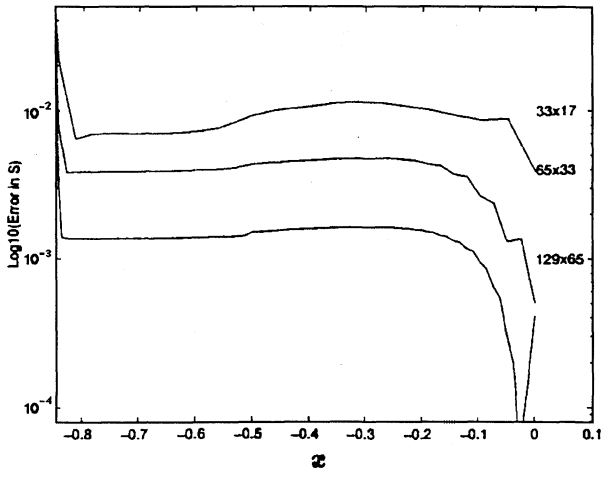


Error in entropy

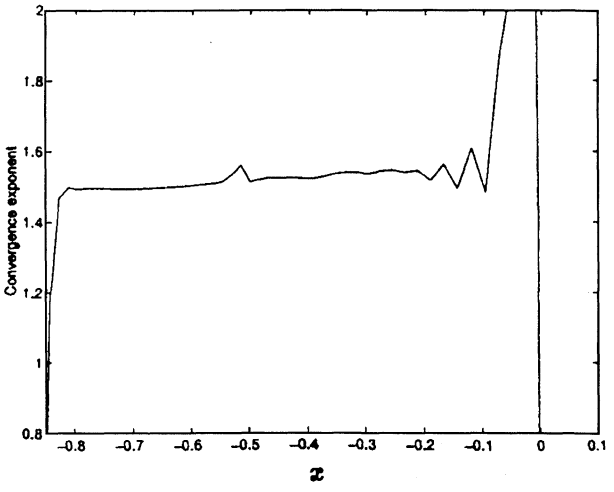


Convergence exponent of Eq. (9)

**Fig. 4 Second-order UNO scheme.**

*2. Spurious Dynamics of TVD Schemes for the Embid et al. Problem*

It has long been observed that the occurrence of residual plateauing is common when TVD and ENO types of schemes are used to time march to the steady state. That is, the initial decrease in the residual levels out and never reaches the convergence tolerance (see Refs. 20, 30, 31, 59, and 60 for discussion). This has often been overcome by ad hoc modification of the flux limiter or similar device in problem regions.

In a recent study, Burton and Sweby[61] investigated this phenomenon using a dynamical systems approach for the one-dimensional scalar test problem of Embid et al.,[62]

$$u_t + \left(\tfrac{1}{2}u^2\right)_x = g(x)u = (6x-3)u, \qquad x \in (0,1) \tag{11a}$$

with boundary conditions

$$u(0) = 1, \qquad u(1) = -0.1 \tag{11b}$$

This equation with the flux function $f(u) = u^2/2$ has the property that there are two entropy satisfying steady solutions consisting of stationary shocks jumping between the two solution branches

$$u^l(x) = 3x(x-1) + 1 \tag{12a}$$

$$u^r(x) = 3x(x-1) - 0.1 \tag{12b}$$

For this problem the two possible solutions consist of a single shock, either approximately at $x_1 = 0.18$ or $x_2 = 0.82$. It can then be shown[62] that the solution with a shock at $x_1$ is stable to perturbations whereas the solution with a shock at $x_2$ is unstable.

Embid et al.[62] solved Eq. (11) using three different methods: the first-order implicit upwind scheme of Engquist and Osher, its second-order counterpart, and the second-order explicit MacCormack scheme. All three schemes used time stepping as a relaxation technique for solving the steady-state equation. The initial conditions were taken to follow the solution branches (12) from the boundary values with a single jump between the two branches. The results obtained showed, although the implicit schemes allowed large time steps and hence fast convergence, if the initial jump was taken too near the unstable shock position $x_2$, then for some ranges of Courant number,

$$c = u(\Delta t/\Delta x) \tag{13}$$

the schemes would converge to the physically unstable shocks. This phenomenon was studied both for these three schemes and a variety of flux limited TVD schemes[63] in Burton and Sweby,[61] where not only the full problem was studied but also a reduced $2 \times 2$ system was investigated using a dynamical system approach. We summarize this investigation here.

The schemes investigated were explicit and implicit versions of the Engquist–Osher and TVD flux limiter schemes using the minmod, van Leer, van Albada, and superbee flux limiters. For the time discretization, explicit Euler was used for the explicit implementations, whereas linearized implicit Euler was used for the implicit computations. For the second-order flux limiter schemes the Jacobian matrix for the implicit part was taken to be that of the first-order Engquist–Osher to allow easy inversion.

Denoting $f$ as the convection flux, the schemes for the explicit Euler and linearized implicit Euler are

$$u_j^{n+1} = u_j^n - \lambda\Delta_-\left(f_{j+1}^- + f_j^+\right) + \Delta t g(x)u_j^n$$
$$- \tfrac{1}{2}\lambda\Delta_-\left[\phi\left(r_j^+\right)\left(\Delta f_{j+\frac{1}{2}}\right)^+ - \phi\left(r_{j+1}^-\right)\left(\Delta f_{j+\frac{1}{2}}\right)^-\right] \tag{14}$$

$$J\left(u_j^n\right)\left[u_j^{n+1} - u_j^n\right] = -\lambda\Delta_-\left(f_{j+1}^- + f_j^+\right) + \Delta t g(x)u_j^n$$
$$- \tfrac{1}{2}\lambda\Delta_-\left[\phi\left(r_j^+\right)\left(\Delta f_{j+\frac{1}{2}}\right)^+ - \phi\left(r_{j+1}^-\right)\left(\Delta f_{j+\frac{1}{2}}\right)^-\right] \tag{15}$$

respectively, where $f_j^{\pm}$ are the Engquist–Osher numerical fluxes

$$f_j^+ = f(\max(u_j, 0)) \tag{16a}$$

$$f_j^- = f(\min(u_j, 0)) \tag{16b}$$

The flux differences are given by

$$\left(\Delta f_{j+\frac{1}{2}}\right)^+ = -\left[f_{j+1}^+ - f(u_{j+1})\right], \qquad \left(\Delta f_{j+\frac{1}{2}}\right)^- = \left[f_j^- - f(u_j)\right] \tag{17}$$

and the solution monitors by

$$r_j^{\pm} = \left[\frac{\left(\Delta f_{j-\frac{1}{2}}\right)^{\pm}}{\left(\Delta f_{j+\frac{1}{2}}\right)^{\pm}}\right]^{\pm 1} \tag{18}$$

Finally, $J$ is the Jacobian matrix, and the flux limiter $\phi(r)$ is one of the following.

First-order Engquist–Osher (E–O) scheme:

$$\phi_0(r) = 0 \tag{19}$$

The minmod limiter:

$$\phi_1(r) = \max(0, \min(r, 1)) \tag{20}$$

Roe's superbee limiter:

$$\phi_2(r) = \max(0, \min(2r, 1), \min(r, 2)) \tag{21}$$

Van Leer's limiter:

$$\phi_{\mathrm{VL}}(r) = \frac{r + |r|}{1 + |r|} \tag{22}$$

Van Albada's limiter:

$$\phi_{\mathrm{VA}}(r) = [(r + r^2)/(1 + r^2)] \tag{23}$$

Numerical experiments reported in Burton and Sweby[61] used a grid spacing of $\Delta x = 0.025$ with initial conditions consisting of a single

**Table 1 Convergence regions for the explicit schemes**

| Scheme | $c_i$ | $c_j$ |
|---|---|---|
| E–O | 0.65 | 0.9 |
| Minmod | 0.5 | 0.75 |
| Superbee | —— | 0.7 |
| van Leer | 0.6 | 0.7 |
| van Albada | 0.6 | 0.7 |

**Table 2 Convergence regions for the implicit schemes**

| Scheme | Converges to $x_1$ | Converges to $x_2$ |
|---|---|---|
| E–O | $c < 11$ | $c \geq 22.5$ |
| Minmod | $c < 11$ | $c \geq 21.5$ |
| Superbee | $c < 11$ | —— |
| van Leer | —— | —— |
| van Albada | $c < 11$ | $c \geq 22.5$ |

jump between the solution branches (12) near either the stable shock ($x_1$) or the unstable shock ($x_2$). The convergence criterion used was the following bound on the residual:

$$\sum_j |u_j^{n+1} - u_j^n| \leq 10^{-15} \tag{24}$$

with an upper limit of 2000 iterations being performed.

The results of applying these schemes to problem (11) largely echoed those reported by Embid et al.[62] For the explicit schemes convergence, when it occurred, was to the stable shock. It was found that there were regions of Courant number ($c \leq c_i$) for which the schemes converged, regions ($c_i < c < c_j$) for which convergence did not take place using Eq. (26) within 2000 iterations, and regions ($c > c_j$) for which the schemes were unstable. This is summarized in Table 1. The absence of an entry corresponds to residual plateauing.

Notice that for the superbee flux limiter there was no range of Courant numbers for which the scheme converged. Closer inspection reveals residual (defined as $r^n = |u^{n+1} - u^n|$) plateauing at around $10^{-3}$. For the other schemes, when $c_i < c < c_j$, the nonconvergence observed arises from a similar process, except that the residual does not necessarily level out completely, but decreases at a very gradual rate, resulting in very slow convergence.

The implicit scheme experiments revealed that the choice of initial conditions could cause convergence to the unstable shock for certain ranges of Courant number. For an initial jump near the stable shock, the schemes (with the exception of the van Leer limiter) converge to the stable shock for $c < 11$. However, for an initial discontinuity near the unstable shock, convergence could sometimes be toward the unstable shock. The situation is summarized in Table 2, where again the absence of an entry corresponds to residual plateauing.

To gain further insight into this problem, Burton and Sweby considered a reduced problem consisting of two free points at one of the shocks, with exact solution values being imposed as boundary conditions on either side. This then leads to a two-dimensional dynamical system, which, although obviously a gross simplification of the full problem, was hoped to still maintain some of the qualitative behavior.

The situation is as shown in Fig. 5, where the free points are $X$ and $Y$, the remaining points being ($U_{ll}$, $U_l$, $U_{rr}$, and $U_r$) set at exact analytic values to provide boundary conditions. Two such values are needed on either side to provide the necessary information for the flux limiters. Substitution of these points into the numerical scheme then leads to a two-dimensional system. For example, the explicit E–O scheme yields

$$X^{n+1} = X^n - (\Delta t/40)\big[f^-(Y^n) + f^+(X^n) - f^-(X^n) - f^+(U_l)\big] - \tfrac{39}{20}\Delta t X^n \tag{25a}$$

$$Y^{n+1} = Y^n - (\Delta t/40)\big[f^-(U_r) + f^+(Y^n) - f^-(Y^n) - f^+(X^n)\big] - \tfrac{36}{20}\Delta t Y^n \tag{25b}$$

where a step size of $\Delta x = \frac{1}{40}$ has been used.

**Table 3 Analytical fixed points of the reduced system**

| | At stable shock | | | At unstable shock | | |
|---|---|---|---|---|---|---|
| Scheme | $X$ | $Y$ | Stable | $X$ | $Y$ | Stable |
| Explicit E–O | 0.36 | −0.47 | $\Delta t < 0.057$ | 0.40 | −0.32 | —— |
| | | | | 0.52 | 0.26 | $\Delta t < 0.1043$ |
| | | | | −0.29 | −0.53 | $\Delta t < 0.1031$ |
| Implicit E–O | 0.37 | −0.48 | $\forall \Delta t$ | 0.40 | −0.32 | $\Delta t > 1.0585$ |
| | | | | 0.52 | 0.26 | $\forall \Delta t$ |
| | | | | −0.29 | −0.53 | $\forall \Delta t$ |

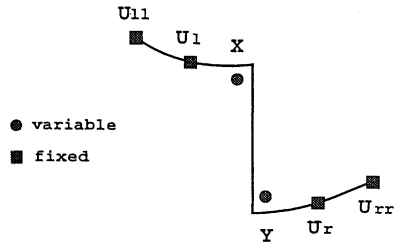


**Fig. 5 Grid points of the reduced Embid et al.[62] problem.**

For the first-order explicit and implicit schemes some analysis on the reduced problem can be performed. Table 3 summarizes the findings. Note that for both schemes spurious asymptotes are introduced by the simplification of the problem. These both have $X$ and $Y$ of the same sign and would not be tolerated for the full problem. It is only the proximity of the boundary conditions for the reduced problem that allow them to exist as asymptotes. However, the remaining asymptotes and their stability agree well with numerical results obtained for the full problem.

Analytical results could only be obtained for the first-order scheme, and so numerical experiments were performed for the flux limiter schemes. These consisted of generating bifurcation diagrams for $X$ and $Y$ against $\Delta t$ and the plotting of basins of attraction in the $(X, Y)$ plane for fixed values of $\Delta t$. The explicit schemes were shown to possess no spurious dynamics below their respective stability limits, apart from that introduced by the simplification of the problem, i.e., outside of the quadrant ($X > 0, Y < 0$). As $\Delta t$ was increased above the stability limit the schemes entered a period of bifurcation and chaos accompanied by a dramatic shrinkage in the numerical basins of attraction.

The dynamics of the implicit schemes at the unstable shock showed the falsely stable steady state becoming stable for large values of $\Delta t$. For all of the limiters tested the stabilizing of the steady state was accompanied by the introduction of additional, spurious (period two) asymptotes. These spurious solutions caused a reduction in size of the basin of the falsely stable steady state. The fact that the more compressive limiters took longer to recover from the effects of the spurious asymptotes seems a possible cause of the phenomenon of residual plateauing experienced in the full problem. Because of limited space, see Burton and Sweby[61] for the illustrations.

It must be realized that although the residual plateauing illustrated is around the physically unstable shock (to which we would usually not wish to converge), the fact that it is not a repelling phenomenon will in itself have repercussions on convergence to the correct, physically stable shock. We conclude this section by emphasizing that the reduced problem indicated a possible cause for residual plateauing. However, for certain situations the dynamics of the full problem does not coincide precisely with that of the reduced problem.

### 3. *Dynamics of Grid Adaption*

Consider a model convection–diffusion equation of the form

$$u_t + f(u)_x = \epsilon u_{xx} \tag{26}$$

with the linear case, $f(u) = u$ and the nonlinear case, $f(u) = \frac{1}{2}u^2$ (the Burgers equation), respectively. The boundary conditions for the linear case are $u(0, t) = 0$ and $u(1, t) = 1$ and for the nonlinear case are $u(0, t) = 1$ and $u(1, t) = -1$. These boundary conditions result in steady-state solutions of a boundary layer at $x = 1$

and a viscous shock at $x = \frac{1}{2}$, respectively. In both cases the steepness of the feature is governed by the diffusion coefficient parameter $\epsilon$. Besides its steepness feature, one of the main reasons for considering the linear convection–diffusion equation is to show that grid adaptation alone and/or nonlinear schemes such as TVD schemes can introduce unwanted dynamics to the overall solution procedure. The authors realize that model (26) is not the best model to illustrate the dynamics of the studied schemes because the model is not stable under perturbations. However, it serves to show what type of spurious numerics would occur under such an environment.

One common criterion used for grid adaptation is the equidistribution of a positive definite weight function $w(x, t)$, often taken to be some monitor of the numerical solution $u(x, t)$ of the underlying PDE. A grid $x_0 < x_1(t) < \cdots < x_{J-1}(t) < x_J$, where $x_0$ and $x_J$ are fixed, equidistributes $w(x, t)$ (at time $t$) if

$$\int_{x_{j-1}}^{x_j} w(x,t)\,dx = \int_{x_j}^{x_{j+1}} w(x,t)\,dx = \frac{1}{J}\int_{x_0}^{x_J} w(x,t)\,dx \quad (27)$$

for $j = 1, \ldots, J$. A one-parameter family of weight functions

$$w(x,t) = \sqrt{1 - \alpha + \alpha u_x^2(x,t)}, \qquad \alpha \in [0, 1] \quad (28)$$

can be chosen where $\alpha = \frac{1}{2}$ corresponds to equidistribution in the arc length and $\alpha = 0$ yields a uniform grid. Approximating $w(x, t)$ to be constant in each interval $(x_{j-1}, x_j)$ yields

$$\left(\sqrt{1 - \alpha + \alpha u_x^2}\right)_{j-\frac{1}{2}} (x_j - x_{j-1}) = \left(\sqrt{1 - \alpha + \alpha u_x^2}\right)_{j+\frac{1}{2}} (x_{j+1} - x_j) \quad (29)$$

Given a numerical solution of the PDE we can approximate the derivatives by

$$u_x|_{j-\frac{1}{2}} \approx \frac{u_j - u_{j-1}}{x_j - x_{j-1}} \quad (30)$$

Equation (29) is nonlinear in $\{x_j\}$ if we use Eq. (30). However, Eq. (29) is linear in $\{x_j\}$ if $\{x_j\}$ in Eq. (30) uses the existing grid. In this case we can solve the tridiagonal system (29) for a new set of $\{x_j\}$ to obtain an updated grid.

Given a set of initial data and an initial grid, the procedure is to numerically solve the PDE and Eq. (29) in a time-lagged manner. We use nodal placement and the $\ell_2$ norm of the solution to illustrate our results. We use the previous time step value for $x_j$ in Eq. (30) to achieve a linear tridiagonal system for the updated grid in Eq. (29). Our preliminary study shows that the solution procedures of Ren and Russel[64] and Budd et al.[65] in solving the coupled PDE and Eq. (29) are less stable than the present linearized form. Also see Neil[66] for a similar study and conclusion. The regridding strategy adopted was to regrid after every time step of the PDE method, either interpolating updated solution values from the old grid or performing no adjustment at all due to grid movement. This latter approach in effect presents the PDE method with new initial data to the problem at each step.

The dynamics of the preceding one-parameter family of mesh equidistribution schemes coupled with different spatial and time discretization were studied numerically in Sweby and Yee[41] and Yee and Sweby[23] using the described numerical procedure. The spatial discretizations include three-point central, second-order upwind and second-order TVD schemes. The time discretizations include explicit Euler, R–K 2 and R–K 4, and the linearized implicit Euler methods. In a parallel study, Budd et al.[67] made use of the AUTO computer bifurcation package[68] to obtain bifurcation diagrams for similar grid adaptation methods for the steady part of the described PDEs with a different form than Eq. (29). However, the dependence on known solutions of the discretized PDEs and grid equations as starting values limits its usage. In Sweby and Yee[41] we utilize the power of the highly parallel Connection Machine CM-5 to undertake a purely numerical investigation into the dynamics of the time-marching adaptive procedure.

We divided a chosen parameter space, e.g., $\epsilon$, into 512 equal intervals, with all other parameters ($\alpha$, $\Delta t$, initial data) fixed. For each chosen parameter value, we iterated the discretized PDE and the grid function, in general, 4000 steps (8000 steps for explicit methods) to allow the solution to settle to an asymptotic state. Then we performed a series of time step/regridding stages, during which we investigated the dynamics by producing an overlaid plot of the $\ell_2$ norms of the numerical solution and the grid distribution at each step. This resulted in a bifurcation type diagram or the grid displacement diagram as a function of the physical or discretized parameters. We also performed numerical studies by only preiterating the discretized PDEs to the steady state for a fixed grid before solving both the discretized PDE and the grid adaptation function. We found in most cases the solution process is less stable and more likely to get trapped in a spurious mode than in the aforementioned process.

For this study, we took into consideration the grid density, an even and odd number of nodes, and whether or not there is interpolation after each regridding. The grid density studies consist of 4, 5, 6, 9, 10, 19, 20, 49, and 50 grid points. There is no apparent sign of even or odd grid dependence. The resolution and stability of TVD schemes are also grid independent. However, the central difference scheme experienced instability more often for coarser grids, and the second-order upwind is slightly more stable, with better resolution than the central scheme. As expected, the stable time step required for the explicit methods was orders of magnitude lower than that for the implicit method. For the TVD schemes, comparison of the dynamical behavior of the five limiters of Eq. (3.50) of Yee[20] was performed. Four of the limiters are the same as Eqs. (19–23). Because of the simplicity of the PDEs, their dynamical behavior is similar, although there were slight differences in the stability and resolution. Because of space limitations, we summarize the results without presenting the actual computational figures. Interested readers should refer to our original papers for details. The following summarizes the results of this subsection.

## V. Summary

We consider separately the cases with and without interpolations. The term scheme from here on means the overall adaptive scheme procedure.

**Case A**

In the no interpolation case for the linear problem, the behavior of the adaptive TVD schemes is similar to that of the classical shock-capturing methods. As opposed to the uniform grid case, the adaptive TVD schemes without interpolations behave rather poorly in terms of stability and allowable $\epsilon$ values (see Figs. 11 and 12 of Yee and Sweby[24]). The solutions refuse to settle down for larger $\Delta t$ and/or smaller $\epsilon$. For the nonlinear problem, the behavior of the adaptive TVD schemes is similar to that of the uniform grid case. The range of allowable $\epsilon$ and $\Delta t$ in terms of stability and convergence rate and settling of the grid distribution are far better than in the linear problem. It appears that for problems with shocks, adaptive TVD schemes favor no interpolation after each regridding (see Figs. 13 and 14 of Yee and Sweby[24]).

**Case B**

In the case with interpolations for the linear problem, as expected, both adaptive TVD schemes and adaptive classical schemes behave in a similar manner in terms of stability and convergence. Adaptive TVD schemes are less stable and have a smaller allowable range of $\epsilon$ than the uniform grid case. Overall, adaptive TVD schemes behave far better than their counterparts without interpolation for the linear problem as can be seen in Figs. 11 and 12 of Yee and Sweby.[24] For the nonlinear problem, the adaptive TVD schemes with interpolations behave like the classical shock-capturing method. They experience nonconvergence of the solution, and the grid distribution cannot settle down for a certain range of $\Delta t$. This can be seen in Figs. 13 and 14 of Yee and Sweby.[24]

It is surprising to see the opposite behavior of the adaptive implicit TVD schemes for the two model PDEs with and without interpolation combinations, especially when the same physical parameters, discretized parameters, and initial data were used.

## VI. Concluding Remarks

We have revealed and isolated some of the causes of spurious phenomena due to the numerics in an attempt to improve the understanding of the effects of numerical uncertainties in CFD in time marching to the steady-state numerical solutions. The nonlinear phenomena and spurious behavior exhibited by the numerics in solving genuinely nonlinear problems reveal many of the limitations, challenges, and barriers in CFD. The knowledge gained so far has already provided some improved guidelines for overcoming the spurious behaviors without resorting entirely to the tuning of computational parameters (see Yee and Sweby[9,24] for some suggestions to minimized spurious numerics). We believe the knowledge of nonlinear behavior of numerical schemes can be a viable complement to the standard guidelines from numerical analysis and CFD practices. Before additional theories are established, we conclude that the safest route is to have some understanding of the nonlinear behavior of the numerical method being used. Knowledge from the recent advances in nonlinear behavior are summarized in Secs. II and III. There remains the challenge of constructing adaptive time step control methods that are suitable yet practical for time marching to the steady states for aeronautical CFD applications. Another even more challenging area is the quest for an adaptive numerical scheme that leads to guaranteed and rapid convergence to the correct steady-state numerical solutions. These two key challenges are particularly important for CFD.

## Acknowledgments

The authors wish to thank their collaborators Andre Lafon and David Griffiths for contributing to their earlier work. In addition, we acknowledge Andre Lafon for the original formulation and the earlier study used in Sec. IV.A; it was presented at the ICFD Conference on Numerical Methods for Fluid Dynamics, April 3–6, 1995, Oxford, England, UK. David Griffiths is thanked as well for his error control results communicated in 1966. The contribution of Sec. IV.B by Bjorn Sjogreen of the Uppsala University is gratefully acknowledged. The private communication from L. Keefe in 1996 on his direct numerical simulation of channel flow is also gratefully acknowledged. We further acknowledge Paul Burton for the computations used in Sec. IV.B.2. Special thanks to Unmeel Mehta for the invitation as an invited speaker to the conference. Thanks also to Unmeel Mehta and Karim Shariff for their critical review of the manuscript.

## References

[1]Aeschliman, D. P., and Oberkampf, W. L., "Experimental Methodology for Computational Fluid Dynamics Code Validation," *AIAA Journal*, Vol. 36, No. 5, 1998, pp. 733–741.

[2]Cosner, R. R., "CFD Validation Requirements for Technology Transition," AIAA Paper 95-2227, June 1995.

[3]Mehta, U., "Guide to Credible Computational Fluid Dynamics Simulations," AIAA Paper 95-2225, June 1995.

[4]Melnik, R. E., Siclari, M. J., Barber, T., and Verhoff, A., "A Process for Industry Certification of Physical Simulation Codes," AIAA Paper 94-2235, June 1994.

[5]Demuren, A. O., and Wilson, R. V., "Estimating Uncertainty in Computations of Two-Dimensional Separated Flows," *Transactions of the American Society of Mechanical Engineers*, Vol. 116, 1994, pp. 216–220.

[6]Marvin, J. G., "Dryden Lectureship in Research, A Perspective on CFD Validation," AIAA Paper 93-0002, Jan. 1993.

[7]Marvin, J. G., and Holst, T. L., "CFD Validation for Aerodynamic Flows—Challenge for the 90's," AIAA Paper 90-2995, Aug. 1990.

[8]Yee, H. C., Torczynski, J. R., Morton, S. A., Visbal, M. R., and Sweby, P. K., "On Spurious Behavior of CFD Computations," AIAA Paper 97-1869, June 1997.

[9]Yee, H. C., and Sweby, P. K., "Nonlinear Dynamics and Numerical Uncertainties in CFD," NASA TM 110398, April 1996.

[10]Jackson, E. A., *Perspectives of Nonlinear Dynamics*, Vol. 1, Cambridge Univ. Press, New York, 1989.

[11]Thompson, J. M. T., and Stewart, H. B., *Nonlinear Dynamics and Chaos*, Wiley, New York, 1986.

[12]Hoppensteadt, F. C., *Analysis and Simulation of Chaotic Systems*, Springer–Verlag, New York, 1993.

[13]Crocco, L., "A Suggestion for the Numerical Solution of the Steady Navier–Stokes Equations," *AIAA Journal*, Vol. 3, No. 10, 1965, pp. 1824–1832.

[14]Moretti, G., and Abbett, M., "A Time-Dependent Computational Method for Blunt Body Flows," *AIAA Journal*, Vol. 4, No. 12, 1966, pp. 2136–2141.

[15]MacCormack, R. W., "The Effect of Viscosity in Hypervelocity Impact Cratering," AIAA Paper 69-354, 1969.

[16]Beam, R. M., and Warming, R. F., "An Implicit Factored Scheme for the Compressible Navier–Stokes Equations," *AIAA Journal*, Vol. 16, No. 4, 1978, pp. 293–302.

[17]Briley, W. R., and McDonald, H., "Solution of the Multidimensional Compressible Navier–Stokes Equations by a Generalized Implicit Method," *Journal of Computational Physics*, Vol. 24, 1977, pp. 372–397.

[18]Steger, J., "Implicit Finite-Difference Simulation of Flow About Arbitrary Two-Dimensional Geometries," *AIAA Journal*, Vol. 16, No. 7, 1978, pp. 679–686.

[19]Lambert, J. D., *Computational Methods in Ordinary Differential Equations*, Wiley, New York, 1973.

[20]Yee, H. C., "A Class of High-Resolution Explicit and Implicit Shock-Capturing Methods," von Kármán Inst. (VKI) for Fluid Dynamics Lecture Series 1989-04, March 6–10, 1989; also NASA TM-101088, Feb. 1989.

[21]Yee, H. C., Sweby, P. K., and Griffiths, D. F., "Dynamical Approach Study of Spurious Steady-State Numerical Solutions for Nonlinear Differential Equations, Part I: The Dynamics of Time Discretizations and Its Implications for Algorithm Development in Computational Fluid Dynamics," NASA TM-102820, April 1990; also *Journal of Computational Physics*, Vol. 97, 1991, pp. 249–310.

[22]Yee, H. C., and Sweby, P. K., "Global Asymptotic Behavior of Iterative Implicit Schemes," NASA RIACS TR 93.11, Dec. 1993; also *International Journal of Bifurcation and Chaos*, Vol. 4, 1994, pp. 1579–1611.

[23]Yee, H. C., and Sweby, P. K., "Dynamical Approach Study of Spurious Steady-State Numerical Solutions for Nonlinear Differential Equations, Part II: Global Asymptotic Behavior of Time Discretizations," NASA Rept. RNR-92-008, March 1992; also *International Journal of CFD*, Vol. 4, 1995, pp. 219–283.

[24]Yee, H. C., and Sweby, P. K., "On Super-Stable Implicit Methods and Time-Marching Approaches," NASA RIACS TR 95.12, July 1995; also *Proceedings of the Conference on Numerical Methods for Euler and Navier–Stokes Equations*, Univ. of Montreal, Montreal, PQ, Canada, 1995.

[25]Lafon, A., and Yee, H. C., "Dynamical Approach Study of Spurious Steady-State Numerical Solutions for Nonlinear Differential Equations, Part III: The Effects of Nonlinear Source Terms in Reaction-Convection Equations," NASA TM 103877, July 1991; also *International Journal of CFD*, Vol. 6, 1996, pp. 1–36.

[26]Lafon, A., and Yee, H. C., "Dynamical Approach Study of Spurious Steady-State Numerical Solutions of Nonlinear Differential Equations, Part IV: Stability vs. Numerical Treatment of Nonlinear Source Terms," ONERA-CERT TR DERAT 45/5005.38; also *International Journal of CFD*, Vol. 6, 1996, pp. 89–123.

[27]Saad, Y., "Preconditioning Krylov Subspace Methods for CFD Applications," *Proceedings of the International Workshop on Solution Techniques for Large-Scale CFD Problems*, edited by W. G. Habashi, Concordia Univ., Montreal, PQ, Canada, 1994.

[28]Turkel, E., "Review of Preconditioning Methods for Fluid Dynamics," *Applied Numerical Mathematics*, Vol. 12, 1993, pp. 257–284.

[29]Wesseling, P., *An Introduction to Multigrid Methods*, Wiley, New York, 1992.

[30]Yee, H. C., "Linearized Form of Implicit TVD Schemes for Multidimensional Euler and Navier–Stokes Equations," *Computers and Mathematics with Applications*, Vol. 12A, 1986, pp. 413–432.

[31]Yee, H. C., Klopfer, G. H., and Montagne, J.-L., "High-Resolution Shock-Capturing Schemes for Inviscid and Viscous Hypersonic Flows," *Journal of Computational Physics*, Vol. 88, 1990, pp. 31–61.

[32]Harten, A., "On High-Order Accurate Interpolation for Non-Oscillatory Shock-Capturing Schemes," *The IMA Volumes in Mathematics and Its Applications*, Vol. 2, Springer–Verlag, Berlin, 1986, pp. 71–106.

[33]Harten, A., and Osher, S., "Uniformly High-Order Accurate Nonoscillatory Schemes I," *SIAM Journal on Numerical Analysis*, Vol. 24, 1987, pp. 279–309.

[34]Engquist, B., and Sjogreen, B., "Numerical Convergence Rate in the Presence of Shocks," Royal Inst. of Technology, Mathematics Rept., Stockholm, Sweden, 1996.

[35]Donat, R., "Studies on Error Propagation for Certain Nonlinear Approximations to Hyperbolic Equations: Discontinuities in Derivatives," *SIAM Journal on Numerical Analysis*, Vol. 31, 1994, pp. 655–679.

[36]Casper, J., and Carpenter, M., "Computational Considerations for the Simulation of Shock-Induced Sound," *SIAM Journal on Scientific and Statistical Computing* (submitted for publication).

[37]Lerat, A., and Sides, J., "Efficient Solution of the Steady Euler Equations with a Centered Implicit Method," *Numerical Methods for Fluid Dynamics III*, edited by K. W. Morton and M. J. Baines, Clarendon, Oxford, England, UK, 1988, pp. 65–86.

[38]Butcher, J. C., *Numerical Analysis of Ordinary Differential Equations*, Wiley, Chichester, England, UK, 1987.

[39]Sweby, P. K., Yee, H. C., and Griffiths, D. F., "On Spurious Steady-State Solutions of Explicit Runge–Kutta Schemes," Dept. of Mathematics, Numerical Analysis Rept. 3/90, Univ. of Reading, Reading, England, UK; also NASA TM 102819, March 1990.

[40]Sweby, P. K., and Yee, H. C., "On Spurious Asymptotic Numerical Solutions of 2 × 2 Systems of ODEs," Dept. of Mathematics, Numerical Analysis Rept. 7/91, Univ. of Reading, Reading, England, UK, 1991.

[41]Sweby, P. K., and Yee, H. C., "On the Dynamics of Some Grid Adaptation Scheme," Proceedings of the 4th International Conf. on Numerical Grid Generation in CFD and Related Fields, Univ. College of Swansea, Swansea, Wales, UK; also NASA RIACS TR 94.02, Feb. 1994.

[42]Dieci, L., and Estep, D., "Some Stability Aspects of Schemes for the Adaptive Integration of Stiff Initial Value Problems," *SIAM Journal on Scientific and Statistical Computing*, Vol. 12, 1991, pp. 1284–1303.

[43]Aves, M. A., Griffiths, D. F., and Higham, D. J., "Does Error Control Suppress Spuriosity?," *SIAM Journal on Numerical Analysis* (to be published).

[44]Lorenz, E. N., "Computational Chaos—A Prelude to Computational Instability," *Physica D*, Vol. 35, 1989, pp. 299–317.

[45]Poliashenko, M., and Aidun, C. K., "Computational Dynamics of Ordinary Differential Equations," *International Journal of Bifurcation and Chaos*, Vol. 5, 1995, pp. 159–174.

[46]Corless, R. M., "Error Backward," *Contemporary Mathematics*, Vol. 172, 1994, pp. 31–62.

[47]Corless, R. M., "What Good Are Numerical Simulations of Chaotic Dynamical Systems?," *Computers and Mathematical Applications*, Vol. 28, 1994, pp. 107–121.

[48]Adams, E., "Periodic Solutions: Enclosure, Verification, and Applications," *Computer Arithmetic and Self-Validating Numerical Methods*, Academic, New York, 1990, pp. 199–245.

[49]Moore, D. R., Weiss, N. O., and Wilkins, J. M., "The Reliability of Numerical Experiments: Transitions to Chaos in Thermosolutal Convection," *Nonlinearity*, Vol. 3, 1990, pp. 997–1014.

[50]Keener, J. P., *Ordinary and Partial Differential Equations*, edited by B. D. Sleeman and R. J. Jarvis, Pitmann Research Notes 157, Longman Sci. Tech., Harlow, 1987, pp. 95–112.

[51]Grebogi, C., Ott, E., and Yorke, J. A., "Crises, Sudden Changes in Chaotic Attractors, and Transient Chaos," *Physica 7D*, 1983, pp. 181–200.

[52]Sweby, P. K., Lafon, A., and Yee, H. C., "On the Dynamics of Computing a Chemically Relaxed Nonequilibrium Flow," ICFD Conf. on Numerical Methods for Fluid Dynamics, April 1995, Oxford, England, UK.

[53]Park, C., "On Convergence of Chemically Reacting Flows," AIAA Paper 85-0247, Jan. 1985.

[54]Workshop on Hypersonics, *Proceedings of the Workshop on Hypersonic Flows for Reentry Problems*, Pt. 2, Antibes, France, 1991.

[55]Mulard, V., and Moules, G., "Non-Equilibrium Viscous Flow Calculations in Hypersonic Nozzles," *Proceedings of the Workshop on Hypersonic Flows for Reentry Problems*, Pt. 2, Antibes, France, 1991.

[56]Seydel, R., *From Equilibrium to Chaos*, Elsevier, New York, 1988.

[57]Engquist, B., and Sjogreen, B., "High Order Shock Capturing Methods," *CFD Reviews*, edited by M. Hafez and K. Oshima, Wiley, New York, 1995, pp. 210–233.

[58]Kreiss, H.-O., and Lundqvist, E., "On Difference Approximations with Wrong Boundary Values," *Mathematics of Computation*, Vol. 22, 1968, pp. 1–12.

[59]Yee, H. C., Warming, R. F., and Harten, A., "Implicit Total Variation Diminishing (TVD) Schemes for Steady-State Calculations," *Journal of Computational Physics*, Vol. 57, 1985, pp. 327–360.

[60]Yee, H. C., and Harten, A., "Implicit TVD Schemes for Hyperbolic Conservation Laws in Curvilinear Coordinates," *AIAA Journal*, Vol. 25, No. 2, 1987, pp. 266–274; also AIAA Paper 85-1513, July 1985.

[61]Burton, P. A., and Sweby, P. K., "A Dynamical Approach Study of Some Explicit and Implicit TVD Schemes and Their Convergence to Steady-State Solutions," Dept. of Mathematics, Numerical Analysis Rept. 5/95, Univ. of Reading, England, UK, 1995.

[62]Embid, P., Goodman, J., and Majda, A., "Multiple Steady States for 1-D Transonic Flow," *SIAM Journal on Scientific Statistical Computing*, Vol. 5, 1984, pp. 21–41.

[63]Sweby, P. K., "High Resolution Schemes Using Flux Limiters for Hyperbolic Conservation Laws," *SIAM Journal on Numerical Analysis*, Vol. 21, 1984, pp. 995–1011.

[64]Ren, Y., and Russell, R. D., "Moving Mesh Techniques Based upon Equidistribution and Their Stability," *SIAM Journal on Scientific and Statistical Computing*, Vol. 13, 1992, pp. 1265–1286.

[65]Budd, C., Huang, W., and Russell, R. D., "Moving Mesh Methods for Problems with Blow-Up," *SIAM Journal on Scientific and Statistical Computing* (to be published).

[66]Neil, B., "An Investigation of the Dynamics of Several Equidistribution Schemes," M.Sc. Dissertation, Dept. of Mathematics, Univ. of Reading, Reading, England, UK, 1994.

[67]Budd, C. J., Stuart, A. M., Koomullil, G. P., and Yee, H. C., "Numerical Solution Behavior of Model Convection-Diffusion BVP with Grid Adaptation," *SIAM Journal of Numerical Analysis* (to be published).

[68]Doedel, E., "AUTO: Software for Continuation and Bifurcation Problems in Ordinary Differential Equations," California Inst. of Technology, Rept., Pasadena, CA, 1986.

J. Kallinderis
*Associate Editor*